PHYSICAL REVIEW E **78**, 036216 (2008)

Dynamics of tidal synchronization and orbit circularization of celestial bodies

Bruno Escribano,[1] Jozsef Vanyo,[2] Idan Tuval,[3] Julyan H. E. Cartwright,[1] Diego L. González,[4] Oreste Piro,[5] and Tamás Tél[2]
[1]*Instituto Andaluz de Ciencias de la Terra, CSIC–Universidad de Granada, Campus Fuentenueva, E-18071 Granada, Spain*
[2]*Institute for Theoretical Physics, Eötvös University, P.O. Box 32, H-1518 Budapest, Hungary*
[3]*Department of Applied Mathematics and Theoretical Physics, University of Cambridge, Cambridge CB3 0WA, United Kingdom*
[4]*Musical and Architectural Acoustics Laboratory, FSSG-CNR, I-30124 Venezia, Italy*
[5]*Departamento de Física e Instituto de Física Interdisciplinar y Sistemas Complejos IFISC (CSIC-UIB), Universitat de les Illes Balears, E-07122 Palma de Mallorca, Spain*
(Received 3 December 2007; revised manuscript received 19 August 2008; published 18 September 2008)

We take a dynamical-systems approach to study the qualitative dynamical aspects of the tidal locking of the rotation of secondary celestial bodies with their orbital motion around the primary. We introduce a minimal model including the essential features of gravitationally induced elastic deformation and tidal dissipation that demonstrates the details of the energy transfer between the orbital and rotovibrational degrees of freedom. Despite its simplicity, our model can account for both synchronization into the 1:1 spin-orbit resonance and the circularization of the orbit as the only true asymptotic attractors, together with the existence of relatively long-lived metastable orbits with the secondary in $p:q$ synchronous rotation.

DOI: 10.1103/PhysRevE.78.036216 PACS number(s): 05.45.Xt, 05.45.Gg, 95.10.Ce, 96.15.De

I. INTRODUCTION

What is the dynamical origin of the fact that the Moon presents the same hemisphere facing perpetually toward the Earth? The other large moons of the solar system also have their rotations synchronized with their orbits, and Pluto and Charon are mutually locked in this way. All of these celestial bodies are in 1:1 spin-orbit resonance. The rotation of one planet, Mercury, is also synchronized with its orbit around the Sun, but it performs three rotations every two orbits, and thus, unlike the former instances, is locked not in 1:1, but instead in 3:2 resonance [1]. Similar synchronization phenomena are thought to occur too in solar systems with so-called "hot Jupiters" or short-period planets [2], and in systems of binary stars [3], whose orbits also evolve to become circular. All these instances are clearly a consequence of a spin-orbit interaction brought about by the gravitational torque exerted by the larger primary body on the smaller secondary body elastically deformed by the differential gravity combined with the corresponding tidal friction induced in the secondary. The phenomenon has long been studied [4,5], but existing models [6–10] are designed for quantitative analysis of a specific instance or a particular part of the problem, and are correspondingly complicated; the details obscure the basic mathematical structure of the dynamical system.

Here we take the opposite course: in this paper we study the simplest possible system that displays tidal synchronization and orbit circularization with a minimal model that takes into account only the essential ingredients of tidal deformation and dissipation in the secondary body. In our qualitative dynamical-systems approach, without including the full panoply of details, we treat in a self-consistent way the temporal evolution of the eccentricity and the energy flow from orbital to rotational motion, important ingredients to understand the long-term evolution of the orbit. Despite its simplicity, our model can account for both synchronization into the 1:1 spin-orbit resonance and the circularization of the orbit as the only true asymptotic attractors, together with the existence of relatively long-lived metastable orbits with the secondary in $p:q$ (coprime integers) synchronous rotation.

From the point of view of dynamical-systems theory, this phenomenon of synchronization is of even broader interest than its application to celestial dynamics because it belongs to a relatively little studied class of dissipative systems that contain an embedded submanifold of conservative motion. Other examples, unrelated in physical origin but with this same mathematics, are the dynamics of neutrally buoyant particles in incompressible fluid flows [11], the bailout embedding of volume-preserving and Hamiltonian dynamics [12], and strategies to control Hamiltonian systems [13].

II. METHODS

We model an extended secondary body of mass m by two point masses of mass $m/2$ connected with a damped spring; see Fig. 1(a). This composite body moves in the gravitational field of a primary of mass $M \gg m$ located at the origin. In this

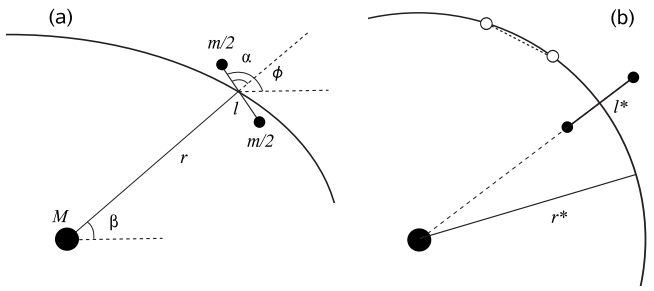

FIG. 1. (a) Instantaneous configuration of the system given by the generalized coordinates r, β, l, and ϕ. The relative angle $\alpha = \phi - \beta$ is indicated. (b) Two conservative synchronized configurations on a circular orbit of radius r^*. That of the black circles, corresponding to a solution of Eq. (3) with the spring stretched ($l^* > l_0$), is stable. The other of white circles and the spring relaxed is unstable.

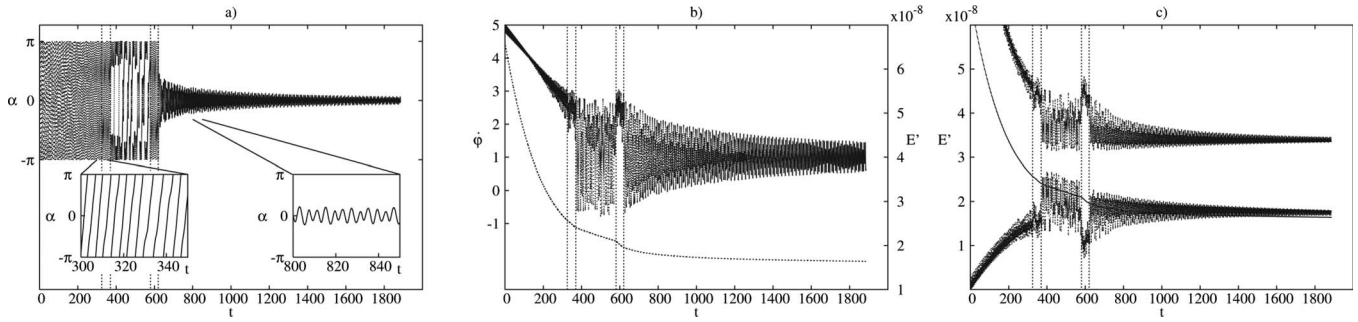

FIG. 2. (a) Angle α vs time t. (b) Angular velocity $\dot{\phi}$ vs time. The decay of the mechanical energy E (thin line) is also shown. Different subregimes are separated by dashed vertical lines; note that the energy decay differs between them. (c) Energy of the different subsystems (shifted by constants) vs time. Smooth line: total energy $E'=E+1/2$, lower curve: center-of-mass energy $E'=E_c+1/2$, and upper curve: rotational and vibrational energy $E'=E_r+E_v+3.5\times10^{-8}$ [cf. Eq. (4)]. $\varepsilon_0=0.1$, $\gamma=1.0$, $l_0=10^{-4}$; the initial condition is $\phi(0)=0$, $\dot{\phi}(0)=5$.

simplest case oscillation and rotation of the secondary are assumed to take place in the plane of the Keplerian orbit. We use polar coordinates r,β for the center of mass of the secondary, with l as the instantaneous length of the spring and ϕ the rotational angle characterizing the orientation of the secondary. Both angles β and ϕ are measured from the x axis in an inertial reference frame. The spring is characterized by its spring constant D and rest length L_0. The gravitational interactions of both point masses with the primary are taken into account, but that between the point masses is neglected. To describe the conservative part of the dynamics we construct a dimensionless Lagrangian in terms of the generalized coordinates $\vec{q}=(r,\beta,l,\phi)$:

$$\mathcal{L}=\frac{\dot{r}^2}{2}+\frac{r^2\dot{\beta}^2}{2}+\frac{\dot{l}^2}{8}+\frac{l^2\dot{\phi}^2}{8}+\frac{1}{2r_1}+\frac{1}{2r_2}-\frac{\omega^2}{8}(l-l_0)^2, \quad (1)$$

where $r_i=[r^2+l^2/4+(-1)^i rl\cos(\phi-\beta)]^{1/2}$ is the distance of theu ith component of the secondary to the primary. $\mathcal{L}$ is measured in units of $(mL^2)/(T^2)$, where the unit of length L is chosen to be the major semiaxis a_0 of the initial Keplerian orbit, and the unit of time $T=(a_0^3/fM)^{1/2}$ is $1/(2\pi)$ times the period of the Keplerian orbit. The dimensionless vibrational frequency and natural spring length are $\omega=\sqrt{4D/m}T$ and $l_0=L_0/a_0$. The damping of the spring is introduced via a dimensionless Rayleigh dissipation function:

$$\mathcal{F}(\dot{l})=\frac{1}{4}\gamma\dot{l}^2,$$

where γ is the dimensionless damping constant. The equations of motion are then given by the modified Euler-Lagrange equations [14]

$$\frac{d}{dt}\frac{\partial\mathcal{L}}{\partial\dot{q}_k}-\frac{\partial\mathcal{L}}{\partial q_k}=-\frac{\partial\mathcal{F}}{\partial\dot{q}_k}, \quad k=1,\ldots,4; \quad (2)$$

the set of dimensionless parameters is γ, l_0, ω, and the eccentricity of the initial Keplerian orbit, ε_0. We take the initial conditions at apapsis, the greatest distance of the center of mass of the secondary from the primary on the initial Keplerian ellipse: $r(0)=1+\varepsilon_0$, $\dot{r}(0)=0$, $\beta(0)=0$. This condition, along with the value of the eccentricity ε_0, determines $\dot{\beta}(0)$. $\dot{\phi}(0)$ was chosen in the range (0,5) with $\phi(0)$ typically zero and $\dot{l}(0)=0$, and $l(0)$ was specified as the value corresponding to a steady rotation with angular velocity $\dot{\phi}(0)$ in the absence of any gravitational force. The numerical solution of the equations of motion was carried out with a fourth-order Runge-Kutta method at fixed step size $\Delta t=2\pi/1000$.

Owing to the damping, the only energy-conserving trajectories of the system are those that maintain the distance between the two point masses making up the secondary constant. These trajectories can only be circular and just two configurations for such orbits are possible: either the two bodies travel along the same circular orbit at a constant distance r^* from the primary or they occupy the same radial line while traveling around two different concentric circular orbits; see Fig. 1(b). In the latter case the radii of the two orbits $r_1^*<r_2^*$ must satisfy the balance between the centrifugal, elastic, and gravitational components of the force,

$$\left(\frac{a_0}{r^*}\right)^3 r_i^*=\frac{1}{r_i^{*2}}+(-1)^i\frac{\omega^2}{2}(r_2^*-r_1^*-l_0), \quad (3)$$

where $(a_0/r^*)^{3/2}$ is the dimensionless orbital angular velocity along the asymptotic circular orbit of radius r^*. It is intuitively clear and readily verifiable by solving Eq. (3) that the equilibrium size $l^*=r_2^*-r_1^*$ is greater than l_0, so that the composite secondary body is stretched in this state.

III. RESULTS AND DISCUSSION

Figure 2 shows a numerical computation of the angle α and angular velocity $\dot{\phi}$ of the secondary as a function of time; the behavior seen is typical for all the parameters investigated for initially rapidly rotating secondaries. A strong initial decay is followed by irregular (transiently chaotic) rotation of the secondary. This may be interrupted by trapping into different resonant states in which the ratio of the rotational and orbital periods is a rational number. Although the use of the term "resonant" is typically applied to Hamiltonian problems, we use it here in the context of a weakly dissipative system since these states appear as attractors or metastable attractors. Eventually, a roughly exponential decay sets in toward a steady state. Two qualitatively different regimes can be observed in the time dependence of the angle

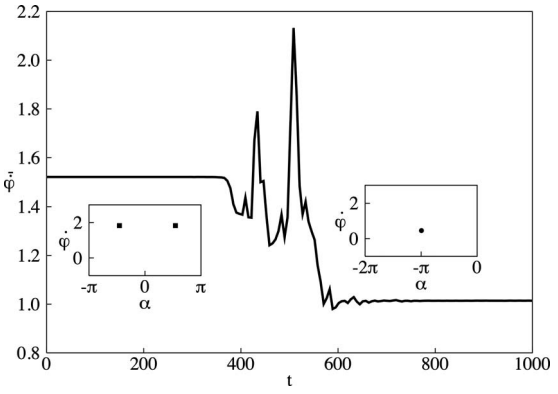

FIG. 3. Average angular velocity $\bar{\dot{\phi}}$ vs time for $\varepsilon_0=0.2$, $\gamma=\omega=10$, $l_0=10^{-4}$ shows the crossover from 3:2 to 1:1 resonance. The initial condition is $\phi(0)=1.2$, $\dot{\phi}(0)=1.0$. The insets show the metastable 3:2 and asymptotic 1:1 attractors on the Poincaré map $\dot{\phi},\alpha$ taken at apapsis. Time is measured in units of T. The transition shown occurs after the system has spent a long time, $t\simeq 4\times 10^7$, in the 3:2 resonance, and is very abrupt, lasting 300 time units, or about 50 periods. The average angular velocity on the first plateau is somewhat larger than 1.5 because the semiaxis has decreased by a few percent by this time.

α in Fig. 2(a): regimes of rotation and of libration, the details of which are exemplified in two insets. The first regime consists of four different subregimes which can best be distinguished on an angular velocity versus time plot. These subregimes are separated by dashed lines in Fig. 2(b). After an initial deceleration phase the angle dynamics is trapped into resonance, a 5:2 resonance in this case. This is followed by an irregular rotation which ends by a further approach to a resonant state, the same one as before in this particular example. The escape from this state occurs in the form of damped oscillations. Figure 2(c) displays how the energy of the different subsystems changes with time. The total dimensionless energy E is split into a center-of-mass energy, a rotational energy, and a vibrational energy $E=E_c+E_r+E_v$ as

$$E_c=\frac{1}{2}(\dot{r}^2+r^2\dot{\beta}^2)-\frac{1}{r},$$

$$E_r=\frac{1}{8}l^2\dot{\phi}^2-\frac{1}{2r_1}-\frac{1}{2r_2}+\frac{1}{r},$$

$$E_v=\frac{1}{8}[\dot{l}^2+\omega^2(l-l_0)^2]. \tag{4}$$

Figure 2(c) demonstrates that in spite of the overall initial decay of energy, the center-of-mass energy increases, i.e., rotation and vibration pump energy into the Keplerian orbit. In the chaotic stage, the subsystem energies E_c, E_r, and E_v all change irregularly, while the total energy decays smoothly, and slower than originally. Around resonances the center-of-mass motion pumps energy into the rotational and vibrational degrees of freedom: a regular center-of-mass motion is an efficient driving of the secondary's internal dynamics. This accumulated vibrational energy quickly dissipates in the last

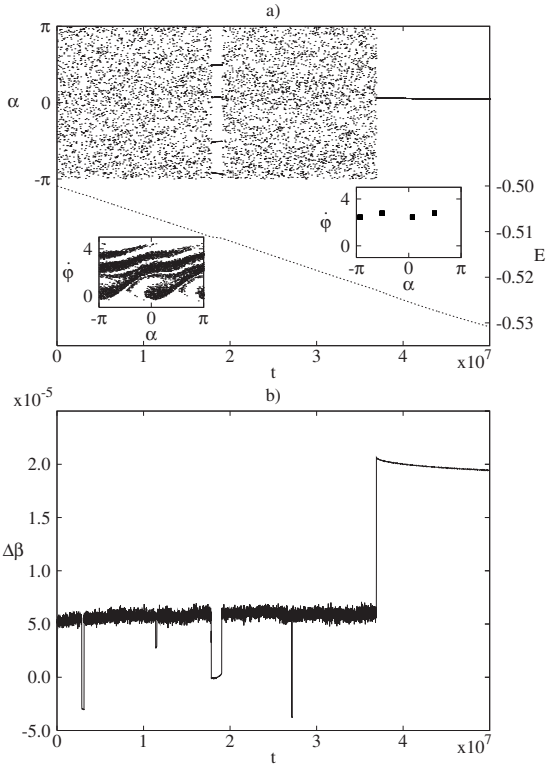

FIG. 4. Long chaotic transients before arrival at 1:1 resonance: (a) Angle α taken at apapsis points vs time and energy E vs time (dashed line) for $\varepsilon_0=0.4$, $\gamma=20$ and initial condition $\phi(0)=0$, $\dot{\phi}(0)=3.5$. The insets show the chaotic and periodic quasi-attractors on a Poincaré map. (b) Periapsis precession $\Delta\beta$ vs time. Note the sudden changes in the periodic windows.

phase. Since the total energy is dominated by the center-of-mass motion, the total decrease of the major semiaxis can be estimated via the Keplerian rule $E^*/E_0=a_0/r^*$, where E_0 and E^* denote the initial and asymptotic total energy.

On intermediate time scales metastable attractors may appear. In particular, the 3:2 resonance may be present for a long period of time. It is, however, asymptotically unstable, and the 1:1 state finally sets in. We see in Fig. 3, which shows the average angular velocity between two successive apapses, that the crossover between the two resonances is rather abrupt, without any long-lasting transients. A change in the parameters or the initial conditions can also lead to a decay direct to 1:1 resonance without an appearance of the metastable 3:2 attractor. Other resonant states can also appear as metastable attractors. Figure 4 presents a case with a 9:4 resonance. Here the transients are very long, with pronounced chaos. Figure 4(a) shows angle α at apapsis versus time; its appearance is that of a bifurcation diagram. A large period-four window appears in the middle of the chaotic regime, and a more detailed investigation reveals further windows. The metastable chaotic and period-four attractors are shown in the insets. Figure 4(b) presents the periapsis precession—the change $\Delta\beta$ of the angle between apsidal points—as a function of time. There is a sudden decrease of this quantity in the periodic windows, but the arrival at the asymptotic 1:1 attractor is marked by a sudden jump upward followed by a slow decrease toward zero.

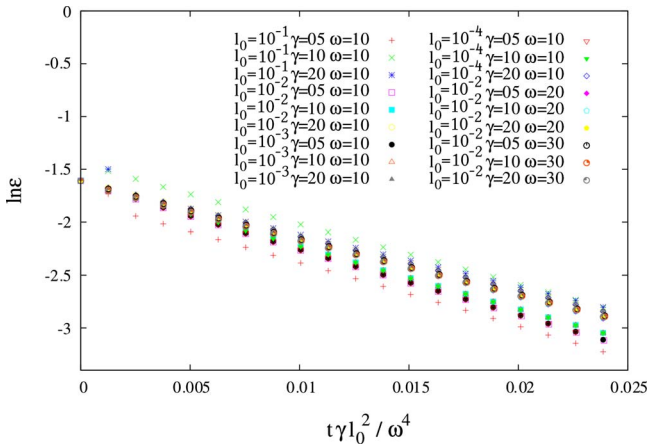

FIG. 5. (Color online) Master curve of the logarithm of eccentricity ε vs rescaled time $t'=t\gamma l_0^2\omega^{-4}$ for initial eccentricity $\varepsilon_0=0.2$, and $\omega=10,20,30$, $l_0=10^{-n}$, $n=1,2,3,4$, and $\gamma=5,10,20$ on a log-linear scale. The initial condition is in all cases $\phi(0)=0$, $\dot{\phi}(0)=4$.

The long-term dynamics always leads to the 1:1 resonance and the energy approaches a constant value; cf. Fig. 2(c). This implies that the full dissipative dynamics converges to a conservative asymptotic state in which the secondary no longer vibrates but behaves as a rigid body orbiting in a circular Keplerian orbit. In order to characterize the approach to this state, we may follow the eccentricity as a function of time. The decay is exponential, but the decay rate varies dramatically with the parameters. The different decay curves, however, follow the same long-term exponential form when plotted as a function of a rescaled dimensionless time t'. In the range $\omega>10$, the scaled time is $t'=t\gamma l_0^2\omega^{-4}$. Figure 5 shows the collapse of a large number of data onto a master curve in this representation. The characteristic relaxation time τ is thus found to scale for $\omega>10$ as $\tau\sim\omega^4/(\gamma l_0^2)$ in the original dimensionless time. The asymptotic state of $\varepsilon=0$ is approached to a good approximation after some 2–3 τ. For $\gamma=1$, $l_0=10^{-4}$, and $\omega=10$, for example, the relaxation time is on the order of 10^{10}. The scaling relation in dimensional form reads

$$\tau_{dim}\sim\frac{1}{\gamma_{dim}}\frac{4^2D^2}{m^2}\frac{a_0^6}{f^2M^2}\frac{a_0^2}{L_0^2}=\frac{1}{\gamma_{dim}}\left(\frac{T_{orb}}{T_{osc}}\right)^4\left(\frac{a_0}{L_0}\right)^2,$$

where T_{osc} is the period of oscillation and T_{orb} the orbital period of the secondary. For a given material composition of the secondary, γ_{dim} and the speed of the elastic waves $c\sim L_0/T_{osc}$ are constants, and the despinning time depends strongly on the size of the secondary and its distance to the primary, which is why large moons are locked to their planets but most planets are not locked to the Sun. This scaling illustrates an interesting feature of the tidal problem: the relaxation time γ_{dim}^{-1} of the isolated oscillator is increased by several orders of magnitude owing to the broad separation of length scales and frequencies. In order to be dissipated by the damping, the energy must be transferred from the orbital and rotational Hamiltonian degrees of freedom to the vibrational one, and this transfer, mediated by the tidal forces, is rather inefficient if the secondary is small. This inefficiency suggests the interesting idea of modeling the secondary in an increasingly complex way as an ensemble of masses linked with conservative—perhaps nonlinear—springs. This might allow for the spontaneous appearance of tidal dissipation as the energy injected by the orbit into the secondary as internal energy thermalizes faster than the time it takes to be fed back into the orbit, and could allow for tidal synchronization and circularization even when no damping at all is present in the secondary if the number of internal degrees of freedom were large enough.

We have introduced here a minimal model that displays the physics of tidal synchronization and orbit circularization without the complexity of an extended body. As the simplest member of a family of models, extensions could eventually include the addition of a nonzero obliquity of the spin axis of the secondary; a more complex secondary; and quasiperiodic or chaotic forcing, as in the three-body problem. We shall develop these ideas in future work.

We acknowledge projects OTKA T72037 (Hungary), Hielocris (Spain), the Human Frontier Science Program (I.T.), MCI project CGL-2008-06245-C02-02 (Spain), and the Spanish-Hungarian Binational project TeT ESP-34/2006.

[1] C. D. Murray and S. F. Dermott, *Solar System Dynamics* (Cambridge University Press, Cambridge, England, 1999).
[2] I. Dobbs-Dixon, D. N. C. Lin, and R. A. Mardling, Astrophys. J. **610**, 464 (2004).
[3] R. A. Mardling, Astrophys. J. **450**, 732 (1995).
[4] G. J. F. MacDonald, Rev. Geophys. **2**, 467 (1964).
[5] P. Goldreich and S. Soter, Icarus **5**, 375 (1966).
[6] B. Gladman, D. D. Quinn, P. Nicholson, and R. Rand, Icarus **122**, 166 (1996).
[7] A. Celletti and L. Chierchia, Celest. Mech. Dyn. Astron. **76**, 229 (2000).
[8] A. C. M. Correia and J. Laskar, Nature (London) **429**, 848 (2004).
[9] A. Celletti, C. Froeschle, and E. Lega, Planet. Space Sci. **55**, 889 (2007).
[10] F. A. Rasio, C. A. Tout, S. H. Lubow, and M. Livio, Astrophys. J. **470**, 1187 (1996).
[11] A. Babiano, J. H. E. Cartwright, O. Piro, and A. Provenzale, Phys. Rev. Lett. **84**, 5764 (2000).
[12] J. H. E. Cartwright, M. O. Magnasco, and O. Piro, Phys. Rev. E **65**, 045203(R) (2002); Chaos **12**, 489 (2002); J. H. E. Cartwright, M. O. Magnasco, O. Piro, and I. Tuval, Phys. Rev. Lett. **89**, 264501 (2002).
[13] J. H. E. Cartwright, M. O. Magnasco, O. Piro, and I. Tuval, Fluct. Noise Lett. **2**, 161 (2002).
[14] J. V. José and E. J. Saletan, *Classical Dynamics: A Contemporary Approach* (Cambridge University Press, Cambridge, England, 1998).